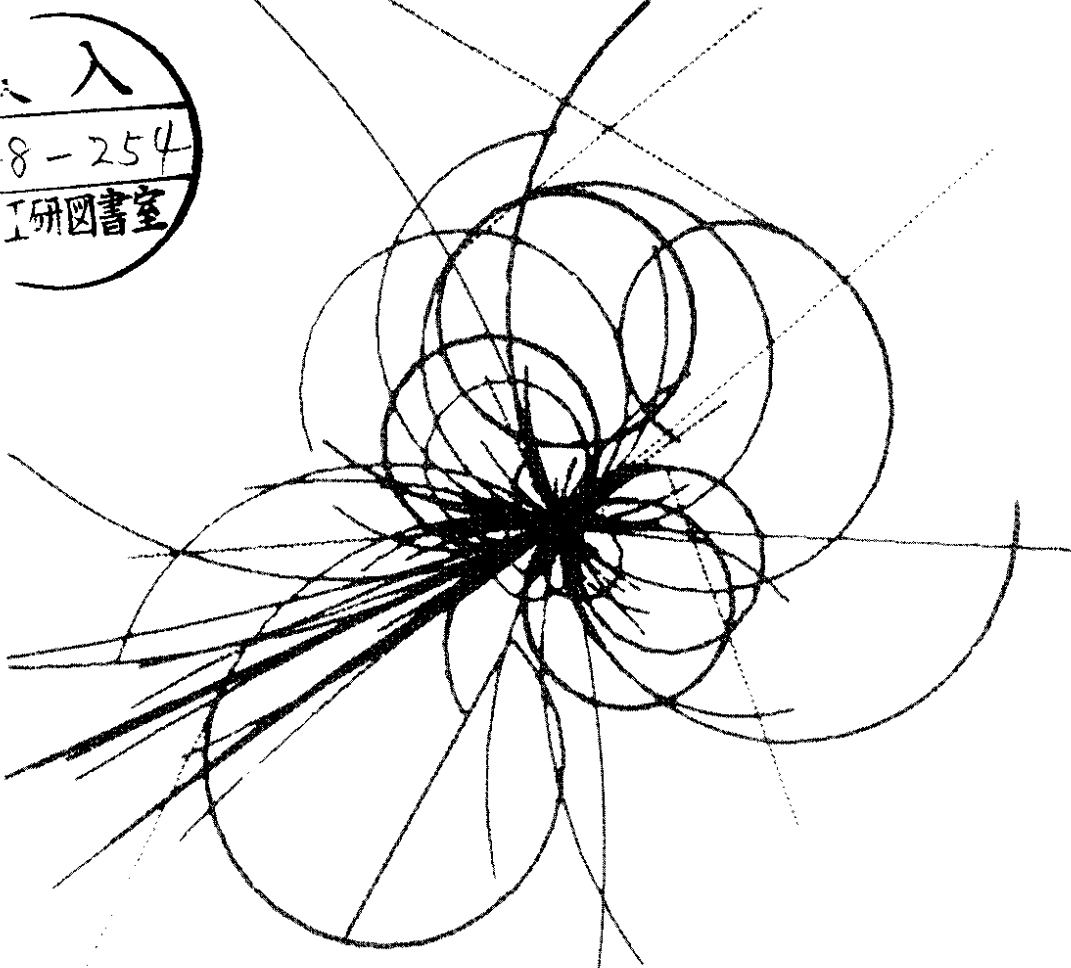


# The Superconducting Super Collider



## Nonlinear Dynamics in the SSC—Experiment E778

Stephen Peggs  
SSC Central Design Group

April 1989

NONLINEAR DYNAMICS IN THE SSC—EXPERIMENT E778\*

Stephen Peggs

SSC Central Design Group†  
Lawrence Berkeley Laboratory  
One Cyclotron Road  
Berkeley, CA 94720

April 1989

---

\* Presented at the Advanced Study Institute on Techniques and Concepts of High Energy Physics, St. Croix, Virgin Islands, 1988.

† Operated by the Universities Research Association, Inc., for the United States Department of Energy.

## NONLINEAR DYNAMICS IN THE SSC — EXPERIMENT E778

Stephen Peggs

SSC Central Design Group\*  
Lawrence Berkeley Laboratory  
1 Cyclotron Road  
Berkeley, CA 94720

### INTRODUCTION

A 1% variation in the cost of an accelerator was not very important forty years ago, when a cyclotron fitted into a single room. Today, when the net cost of an accelerator such as the SSC is measured in billions of dollars, it is much more important to design for an optimum balance between cost and performance. While it is irresponsible to increase the cost of an accelerator more than necessary to make it work "sufficiently" well, it is more irresponsible to construct a machine which almost works, but does not. The problems of large accelerator design lie on the horns of this dilemma. Some aspects of a successful design, such as building in flexibility to enable development in initially unforeseen directions, are almost impossible to quantify. Architectural problems such as these are not addressed here, despite their subtlety and relevance. Neither is the most difficult task addressed — the task of defining what is meant by an accelerator working "sufficiently" well, in terms of needed performance parameters, such as luminosity, lifetime, or linear aperture. Instead, this chapter concentrates on the accelerator physics processes which are expected to limit the performance of the SSC.

There are two broad classes of accelerator physics processes — single particle and collective. Collective effects are caused by the macroscopic electromagnetic fields generated by the numerous circulating charged particles (about  $10^{10}$  particles per bunch). These fields are influenced by the environment, such as the metallic vacuum chamber walls, and act back upon the circulating particles. For example, a single bunch can disrupt itself significantly on one pass through a particular structure in an accelerator. Or, if the fields ring for long enough and have the right frequency, a single bunch can be affected on subsequent turns by the disturbance it laid down on a first turn. Multi-bunch effects occur when a trailing bunch reacts to the ringing fields laid down by preceding bunches.

The performance of the SSC is considered here only in the context of single particle models, in which a test particle circulates a collider for many turns in the presence of static electromagnetic fields. These fields are conceptually divided into linear restoring forces — in which the motion is stable — and nonlinear perturbations. Some sources of nonlinear perturbations are inevitable, in the sense of being designed in (chromatic sextupoles), or of being impossible to design out (beam-beam interactions). Other perturbations are merely random, or accidental, such as imperfections in the magnetic field quality of the

---

\*Operated by the Universities Research Association, Inc. for the Department of Energy.

superconducting magnets. The implicit working hypothesis, which will not be justified, is that single particle effects will dominate collective effects in limiting the performance of the SSC. This is not necessarily true for other accelerators, where collective effects are often crucially important.

Accelerator physics is in good company when it considers the problem of single particle stability in response to nonlinear forces. For example, the question of the stability of the solar system is perhaps the best known and longest standing problem in nonlinear dynamics. Here is a system with an age of order  $10^{10}$  periods (years), which, despite the best efforts of generations of mathematicians, has not been proven to be stable. Rigorous mathematical results are hard to come by in even the simplest nontrivial systems, for example, in the three body problem. More valuable than rigorous results, however, are the analytic languages and tools which classical dynamicists have established in their studies of differential systems — systems which are naturally described by differential equations.

The relatively recent advent of powerful computers caused an explosion in the interest paid to nonlinear problems. Computers, by their cyclical iterative nature, tend to make problems look like difference equations. On the other hand, analytic tools tend to make problems look like differential equations, since they are usually much easier to solve than difference equations, using only a pencil and paper. Which representation is truly appropriate depends on the nature of the system involved. For example, it is natural to represent the solar system as a differential system, since gravity acts smoothly and continuously, while an accelerator is naturally a difference system, since the nonlinear perturbations are usually well represented by brief impulses, separated by lengthy sections of linear motion.

At this point a sceptic might argue that numerical methods do not solve physical systems, they merely demonstrate the behavior of their solutions. An appropriate response to this is to point to the important topic of chaotic behavior in both differential and difference systems, a topic that was historically almost completely neglected by classical dynamicists, because of their lack of difference tools. Exact solutions are impossible when the motion is chaotic. Although Poincare recognised chaos as a distinct phenomenon in differential systems in the late 19th century[1], it was the use of computers in simulating chaotic difference systems that led to a broad appreciation of the ubiquitous nature of the phenomenon, and led indirectly to important formal results. According to the common wisdom, “if the only tool you have is a hammer, all your problems look like nails.”

Despite all the powerful analytic and numerical tools available, it is still impossible to prove the long time scale stability of single particles in the SSC. At this point a physicist resorts to the traditional defense that pragmatism is more important than rigor. The solar system appears to be comfortably stable for  $10^{10}$  periods. Proton storage rings such as the SPS and the Tevatron, with circulation frequency of about 40 kHz and storage times of about one day, are conservative nonlinear systems which are usefully stable for about  $4 \cdot 10^9$  periods. In contrast, the SSC, with a revolution frequency of about 3.5 kHz (the first man-made audio frequency accelerator), needs stability for only about  $3 \cdot 10^8$  turns in order to provide collisions for one day. While the time span of the problem has shortened, the time span of the available tools has lengthened — it is no longer uncommon to follow computer simulations of accelerator models for  $10^6$  turns. Although simulations still fall short of the SSC time scale by about two orders of magnitude, it is reasonable to accept their predictions about the behavior of the SSC, if the simulations agree with the real behavior of existing accelerators operating under relevant nonlinear conditions.

One goal of the E778 nonlinear dynamics experiment is to demonstrate the accuracy of numerical simulations of the Tevatron, when it is put into controlled nonlinear situations which mimic extreme SSC conditions. Another goal is to understand the long and short time scale nonlinear phenomena which are observed. The maximum time scale of the experiment is  $10^6$  turns if limited data is accumulated on every turn, shorter if more data is taken per

turn, or longer if data is taken in periodic bursts. At the time of writing, while anticipating an E778 run in June 1989, it is already possible to say that the short (40,000 turn) time scale behavior is well understood, showing excellent agreement between simulation and experiment[2,3]. Short time scale investigations are now turning to the development of diagnostic and control techniques for the SSC, while the longer time scale investigations are studying phenomenon which, although not critical for SSC performance, have broad interest across the field of nonlinear dynamics[4-7].

The modest goal of this chapter, however, is to give an interested physicist who knows little about accelerators a qualitative description of nonlinear accelerator behavior. Consequently, there is little attempt at rigor, and only some attempt at generality. Models which describe the observed behavior in E778 are emphasised, and some results are shown. Before proceeding to nonlinear discussions, it is necessary to build up a minimum set of accelerator jargon, mostly concerning linear motion. Many references are available if the reader wishes to know more about details of the E778 experiment[8-10], about broader theories of single particle dynamics[11-14], or about the most basic descriptions of accelerator physics[15-22].

### CLOSED ORBITS, LINEAR OSCILLATIONS, AND BETATRON FUNCTIONS

Consider launching a bunch of  $10^{10}$  particles from a reference point for one turn around a storage ring. When the particles return to the reference point, they have traced out trajectories which can be pictured as a dense set of fibers in a rope. Each trajectory is described in detail by two functions,  $X(s)$  and  $Y(s)$ , describing the horizontal and vertical displacements from a design orbit down the center of the beam pipe, as a function of  $s$ , the azimuthal distance around the ring. A trajectory is uniquely labeled by four initial coordinates —  $X(0)$  and  $Y(0)$ , the initial displacements, and  $X'(0) = (dX/ds)(0)$  and  $Y'(0) = (dY/ds)(0)$ , the initial transverse angles. If the magnetic fields encountered are all static, then it can be shown that there is one and only one trajectory, the "closed orbit," which exactly repeats itself. That is, if the circumference of the collider is  $C$ , then

$$\begin{pmatrix} X(C) \\ X'(C) \\ Y(C) \\ Y'(C) \end{pmatrix}_{co} = \begin{pmatrix} X(0) \\ X'(0) \\ Y(0) \\ Y'(0) \end{pmatrix}_{co} \quad [1]$$

The closed orbit is exactly down the center of the beam pipe,  $X_{co}(s) = Y_{co}(s) = 0$ , if all the magnets in the storage ring are perfectly aligned, and if they all have ideal fields. In practice, of course, the closed orbit and the design orbit never quite agree, even in the best of circumstances.

The fibers in the bundle of trajectories are tangled. That is, two trajectories can have the same displacements at some azimuth, and cross. However, if the trajectories are represented in four dimensional phase space as  $(X(s), X'(s), Y(s), Y'(s))$ , then two trajectories may no longer cross, since if they did then the trajectories would become indistinguishable[23]. In almost all of what follows in the rest of this chapter it is possible to ignore the vertical motion, and to consider only purely horizontal motion. The net effect of this simplification here is that the trajectory bundle is now pictured as a set of  $(X, X')$  phase space curves smoothly flowing around the machine, instead of tangled  $(X, Y)$  displacement curves.

Linear motion in horizontal phase space is described by simple matrices. For example, the phase space coordinates leaving a field free drift of length  $L$  are related to the entering coordinates by

$$\begin{pmatrix} X \\ X' \end{pmatrix}_{out} = \begin{pmatrix} 1 & L \\ 0 & 1 \end{pmatrix} \begin{pmatrix} X \\ X' \end{pmatrix}_{in} \quad [2]$$

Motion across a dipole — a magnet with uniform vertical bending field — is essentially the same as across a drift of the same length, since the coordinate frame rotates with the design orbit. (Note that all beam particles are implicitly assumed to have the nominal energy, so that dispersion in the dipoles may be ignored.) In the last kind of linear magnet, a quadrupole of strength  $K$ , motion is described by

$$X'' + K X = 0 \quad [3]$$

A quadrupole is analogous to a thin lens in light optics, and the coordinate transformation is well approximated by

$$\begin{pmatrix} X \\ X' \end{pmatrix}_{\text{out}} = \begin{pmatrix} 1 & 0 \\ \frac{1}{f} & 1 \end{pmatrix} \begin{pmatrix} X \\ X' \end{pmatrix}_{\text{in}} \quad [4]$$

if its length is much less than  $f$ , the focal length of the quadrupole.

Unfortunately, Maxwell's law  $\text{div}(\mathbf{B}) = 0$  leads inevitably to the conclusion that quadrupoles which focus horizontally also defocus vertically, and vice versa. How, then, can a beam be focussed and constrained in two planes simultaneously? The situation is saved by a well known result from light optics, that the net effect of two equal and opposite strength lenses, placed less than their focal length apart, is to focus. Thus a repetitive sequence of FODO cells — Focussing quadrupole, dipole, Defocussing quadrupole, dipole, ... — leads to a net focussing in both planes. The significance of this result was recognised by accelerator physicists in the late 1950's, and was incorporated in the design of the Alternating Gradient Synchrotron, AGS, at Brookhaven, the first “strong focusing” accelerator [24].

The simplest way to describe linear motion is in terms of “normalised” phase space coordinates,  $(x, x')$ , which are related to the “physical” coordinates by the transformation

$$\begin{pmatrix} x \\ x' \end{pmatrix} = \begin{pmatrix} \frac{1}{\sqrt{\beta(s)}} & 0 \\ \frac{\alpha(s)}{\sqrt{\beta(s)}} & \sqrt{\beta(s)} \end{pmatrix} \begin{pmatrix} X \\ X' \end{pmatrix}, \quad \alpha = -\frac{1}{2} \beta' \quad [5]$$

In this frame a linear trajectory is generally solved by

$$\begin{pmatrix} x(s) \\ x'(s) \end{pmatrix} = a_0 \begin{pmatrix} \sin(\phi(s) - \phi_0) \\ \cos(\phi(s) - \phi_0) \end{pmatrix} \quad [6]$$

That is, motion from one azimuth to another is described by a simple rotation, around a circle of constant radius. Motion in physical phase space amounts to progression around a tilted ellipse, with the transformation from ellipse to circle given by equation [5]. The betatron function  $\beta(s)$  which enables this transformation satisfies the differential equation

$$\sqrt{\beta}'' + K(s) \sqrt{\beta} - \beta^{-3/2} = 0 \quad [7]$$

with periodic boundary conditions. The betatron phase  $\phi(s)$  advances smoothly according to

$$\phi' = \frac{1}{\beta} \quad [8]$$

So, in a normalised phase space description of linear motion the trajectory fibers form a bundle which is circularly symmetric. All the fibers turn around the center of the bundle at the same rate, but the rate varies with the azimuthal position.

The betatron function was introduced above in the classical way, through a differential equation which implicitly assumes that the user is interested in the trajectory as a function of  $s$ , the azimuth. It is simpler, and probably more useful, to introduce the beta function in a difference formalism, which assumes that the user is interested in the displacement of a trajectory at a fixed reference point as a function of  $t$ , the integer turn number. This is certainly closer to the experimental setup in E778, in which the displacement of a perturbed beam is measured at two fixed neighboring beam position monitors on tens of thousands of successive turns.

In this perspective linear motion for one turn around a machine is described by multiplying successive drift, dipole, and quadrupole matrices together, in order to get the one turn linear map,  $T$ , where

$$\begin{aligned} \begin{pmatrix} X \\ X' \end{pmatrix}_{t+1} &= T \begin{pmatrix} X \\ X' \end{pmatrix}_t & [9] \\ &= \begin{pmatrix} \cos(2\pi Q) + \alpha \sin(2\pi Q) & \beta \sin(2\pi Q) \\ -\frac{1 + \alpha^2}{\beta} \sin(2\pi Q) & \cos(2\pi Q) - \alpha \sin(2\pi Q) \end{pmatrix} \begin{pmatrix} X \\ X' \end{pmatrix}_t \end{aligned}$$

In normalised coordinates the form of  $T$  is even simpler, corresponding merely to a rotation by  $2\pi Q$ , so that the difference solution is written as

$$\begin{pmatrix} x_t \\ x'_t \end{pmatrix} = a_0 \begin{pmatrix} \sin(2\pi Q t - \phi_0) \\ \cos(2\pi Q t - \phi_0) \end{pmatrix} \quad [10]$$

in small but significant contrast with equation [6]. The betatron tune,  $Q$ , given by

$$2\pi Q = \phi(C) - \phi(0) = \int_0^C \frac{ds}{\beta} \quad [11]$$

is simply the number of twists the trajectory bundle receives in one turn around the accelerator. The solution to the difference equation of motion, equation [10], is only valid for integer  $t$  values. So, the graphical representation of this solution plots one  $(x_t, x'_t)$  dot per turn. Such a representation is called a Poincare "surface of section." Usually, when many of these dots have been plotted, they appear to join together to make a continuous contour — a circle in the case at hand, assuming  $Q$  is irrational.

What happens to this picture when nonlinear perturbations are included? Although everything below is devoted to answering this question in some detail, it is possible to answer the question in one brief paragraph. Usually, the circular contour is simply distorted away from a circle. More rarely, the tune  $Q$  is perturbed to become a rational fraction, say  $m/n$ , resulting in the continuous contour being broken up into  $n$  distinct smooth contours. And sometimes, the sequence of dots do not eventually form a regular contour, but appear to be randomly placed within a bounded chaotic region of the surface of section.

## RESONANCES

Equations [9] and [10] show that only the fractional part of the tune is important for the purposes of discussions with a fixed reference point, because only trigonometric functions of

Q appear. The integer part is dropped from here on, since it is irrelevant. The next refinement is to recognise that the tune is not constant, but is modified by nonlinearities at finite amplitudes, just as the frequencies of near linear oscillators, such as the gravity pendulum, are modified. For example, in one set of E778 conditions which will be referred to below, the tune is approximately

$$Q = Q_0 + k a^2 = 0.418 - 7 \cdot 10^{-4} a^2 \quad [12]$$

where  $Q_0$  is the base, or zero amplitude, tune, and the amplitude of the oscillation,  $a$ , is in millimetres. The strength of the detuning coefficient,  $k$ , depends on the strength of the nonlinearities in the ring.

This detuning means that the rate of twisting in a trajectory bundle changes smoothly with the distance from the center of the bundle. An interesting thing happens when the fractional part  $Q$  is equal, or very close, to a rational fraction. According to equation [12], the tune is equal to  $2/5$  when the amplitude  $a_5$  is about 5.0 millimetres. There are two independent trajectories near this amplitude which exactly repeat themselves after five turns, just as the zero amplitude closed orbit repeats itself exactly after one turn. In the jargon, each of these new trajectories corresponds to five “period five fixed points” on a Poincare surface of section, all with the about the same amplitude  $a_5$ , but with different phases, approximately  $\phi = \phi_0 + i 2\pi/5$ , which are visited in turn. For example, if a trajectory is launched at fixed point  $i = 1$ , after one accelerator turn it returns to point 3, then 5, 2, 4, and then revisits 1 again.

One of these two new trajectories is stable, and the other is unstable. That is, a trajectory launched very close to one of the stable period five fixed points performs linear oscillations around the fixed point, with an amplitude and phase on turn  $t$  which are given by

$$\begin{aligned} \phi_t &= \phi_0 + 2\pi \frac{2}{5} t + \delta\phi \cos(2\pi Q_1 t) \\ a_t &= a_5 + \delta a \sin(2\pi Q_1 t) \end{aligned} \quad [13]$$

The small oscillation tune  $Q_1$  is called the “island tune.” Only a limited range of phases, within  $\pm\delta\phi$  of the fixed points, are visited by this trajectory — this is what is meant by resonant behavior. A trajectory bundle with resonances included is like a cable wound rope — the strands in each component cable rotate around the center of the cable, and each cable rotates in turn around the center of the rope. Figure 1 shows surface of sections plots for a set of trajectories with different initial amplitudes and phases, taken from a numerical simulation of the E778 experiment, with the realistic values used above. Five resonance “islands” are clearly visible.

Resonances are not expected to be important under normal operating conditions of the SSC. It might correctly be objected that it is impossible to avoid resonances completely, since the number line is dense in rational fractions, and there are resonances everywhere. Fortunately, it turns out that the strength of a resonance drops very quickly with its order, so that normally only an insignificant fraction of trajectories are resonant. It is only necessary to avoid low order resonances, with denominators of less than 10, say. Even in the absence of resonances, however, it is desirable to minimise phase space distortions of the surface of section contours. For example, the distinctive triangular shape in figure 1 leads to unacceptable SSC operating conditions at large amplitudes, according to the design criteria laid down in the Conceptual Design Report of the SSC[25]. The amount of distortion is quantified by the quantity smear,  $S$ , where

$$S = \frac{(\langle a_t^2 \rangle - \langle a_t \rangle^2)^{1/2}}{\langle a_t \rangle} \quad [14]$$

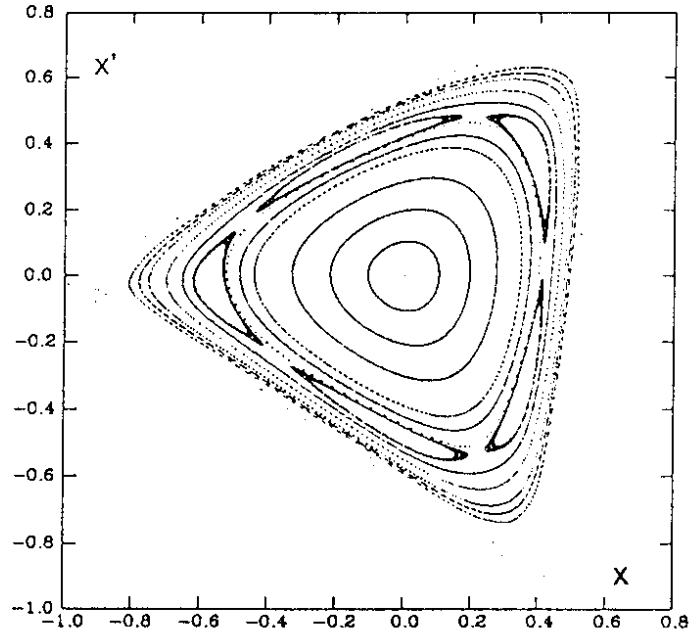


Figure 1. Surface of section plot of several trajectories, from a numerical simulation of the E778 experiment. The value of  $\beta$  is approximately 100 metres, so the five islands at a normalised amplitude of about  $0.5 \cdot 10^{-3} \text{ m}^{1/2}$  have a physical amplitude of about 5.0 millimetres.

where angle brackets,  $\langle \rangle$ , denote an average over turn number. That is, the one dimensional smear is the normalised rms variation in amplitude[26].

## NONLINEAR SOURCES IN ACCELERATORS

### High Order Magnetic Multipoles

The general solution to the Laplace equation for a two dimensional transverse magnetic field is the polynomial

$$B_x + i B_y = B \sum_{n=0}^{\infty} (b_n + i a_n) (X + i Y)^n \quad [15]$$

where  $i = (-1)^{1/2}$ , and  $y$  is the vertical coordinate. This form is convenient for describing magnets in a separated function accelerator, since then only one of the  $b_n$  or  $a_n$  is designed to be non-zero. For example, dipoles, quadrupoles, sextupoles and octupoles are described by single  $b_n$  values, with  $n = 0, 1, 2,$  and  $3$ , respectively — a  $b_n$  magnet has  $2(n + 1)$  poles. Skew magnets, described by  $a_n$  values, have no vertical B-field on the horizontal plane. This breaks a design symmetry of most accelerators, and so skew magnets are mainly used for correction purposes.

Returning to a one dimensional analysis again, the effect of a given pure multipole is to deliver a horizontal angular kick

$$\Delta X' = \frac{1}{(1 + \delta)} \frac{(BL)}{(B\rho)} b_n X^n = \frac{1}{(1 + \delta)} k_n X^n \quad [16]$$

to the trajectory, where  $L$  is the length of the magnet (assumed thin),  $B\rho$  is the rigidity at the nominal storage energy  $E_0$ , and  $\delta = \Delta E/E_0$  represents a small deviation from the nominal energy. All magnets have a geometric strength which varies inversely with the energy. A trajectory with a constant positive  $\delta$  experiences weaker dipoles, and so has a closed orbit which is displaced radially outwards from the center of the magnets by  $\eta(s)\delta$ , where  $\eta$  is called the “dispersion function.” The quadrupoles are also weaker, and this leads to a variation of the tune with energy  $dQ/d\delta$  called the “chromaticity,” which must be compensated in all but the smallest storage rings. The need for this compensation leads to the intentional inclusion of nonlinearities, “chromatic sextupoles,” in storage rings.

Consider a thin sextupole of strength  $k_2$  placed close to a quadrupole of strength  $k_1$ , so that the two may be superimposed. If the displacement is measured as  $Z = X - \eta\delta$ , relative to the displaced closed orbit, then the net kick is approximately

$$\Delta X' \approx k_1 (1 - \delta) (Z + \eta\delta) + k_2 (1 - \delta) (Z + \eta\delta)^2$$

or

[17]

$$\Delta Z' \approx [k_1 + (k_2\eta - k_1)\delta] Z + k_2 [1 - \delta] Z^2$$

in a polynomial expansion where terms above first order in  $\delta$  have been dropped. The coefficient of the first order term in  $Z$  shows that if the sextupole is powered with  $k_2 = k_1/\eta$ , then the net quadrupole effect is constant with respect to first order variations in the energy. If there is a sextupole at every quadrupole, all powered in this way, then the net chromaticity is zero. The price to pay for this correction is the second order term in  $Z$ , a deliberate nonlinear perturbation of approximately constant strength for all trajectories. Chromatic sextupoles are the principle source of nonlinearity in most electron storage rings, but not in large superconducting storage rings like the SSC.

Conventional storage rings use “iron dominated” magnets, with fields below the saturation level in iron, about 2 Tesla. The field is shaped by the iron, and excellent field quality is easily guaranteed by stamping the magnet laminations with the right shape — two flat poles for dipoles, four hyperbolic poles for quadrupoles, and so on. The location of the current carrying conductors is of almost no consequence. On the other hand, the field in superconducting magnets is “conductor dominated” — determined almost entirely by the location of the conductors. If the available current density is infinite, the theoretical solution for the current distribution required to create a pure M-pole field is trivial — a circular current shell of  $I = I_0 \cos(M\theta/2)$ , where  $\theta$  is the angle around the magnet center line. In practice, a significant thickness of superconductor is required to make a dipole field of 6.6 Tesla in the SSC magnets, as shown in Figure 2. It is not possible, even in the ideal design of a two coil layer magnet, to remove all unwanted high order multipole components. This leads to systematic  $b_n$  errors in SSC dipoles. It is mechanically much harder to locate conductors accurately than to stamp out magnet laminations, especially when the profile of the cable is not quite uniform, and the magnetic forces are very strong. Manufacturing variances like this lead to random  $b_n$  and  $a_n$  errors.

Nonetheless, the strongest nonlinear fields in SSC dipoles are due to “persistent currents” on the surface of the superconducting filaments. When Type I superconductors are cooled below their critical temperature, they completely eject any externally imposed magnetic field by generating a compensating surface current. Type II superconductors, such as the Niobium-Titanium commonly used in superconducting magnets, allow partial flux penetration. These persistent currents generate error fields throughout a magnet, with a magnitude which is function, not only of the nominal field strength and distribution, but also of the magnetic history. Persistent current effects are hysteretic.

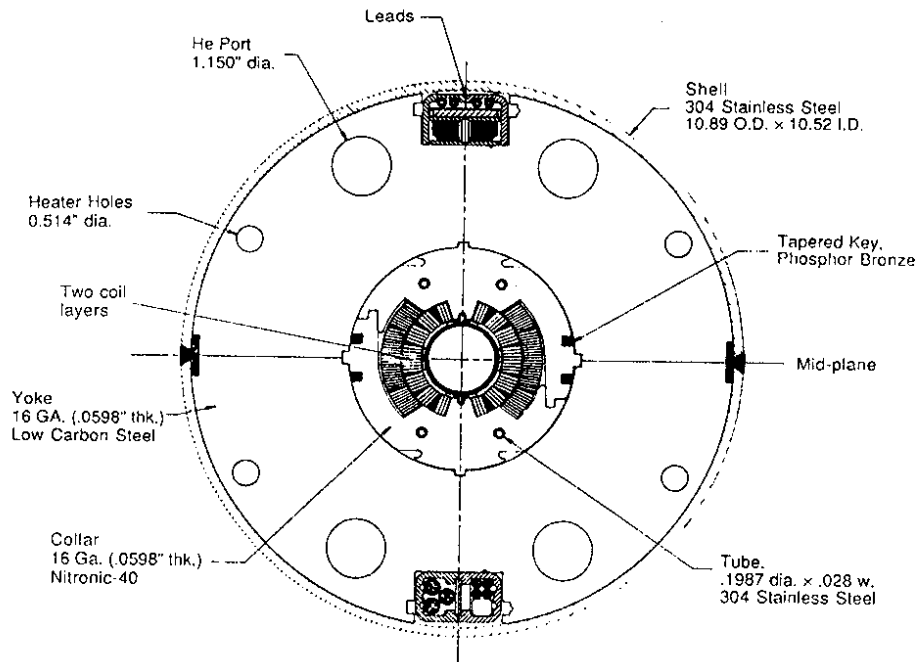


Figure 2. The "cold mass" core of a 6.6 Tesla superconducting SSC dipole. The beam pipe, of 4.0 centimetre inner diameter, is surrounded by a two layer coil which is constrained by a non-magnetic stainless steel collar. The collar, in turn, is constrained by a magnetic steel yoke.

The allowed systematic  $b_n$ 's of the persistent error field have  $n = 2, 4, 6$ , et cetera, with the sextupole and the decapole being of most concern — the persistent sextupoles are far stronger than the chromatic sextupoles at the nominal 1 TeV injection energy of the SSC. Fortunately, the perturbation drops rapidly in strength with increasing energy, and is negligible at 20 TeV. Injection energy is the worst time to have field errors present, because then the beam size is largest — trajectories explore more of the bad field region — and the magnetic rigidity is smallest. To make matters worse, Type II persistent currents decay with time. If uncompensated, this decay causes a continuous drift in the chromaticity while beams are being injected, followed by a rapid large jump when the energy ramp is begun. These problems are foremost in discussions which contemplate an increase of the SSC injection energy to 2 TeV.

#### Beam-Beam

Most contemporary electron and proton storage rings are limited in their performance by the beam-beam effect. Consider a test particle passing through a counter-rotating bunch of particles at a nominal collision point of a storage ring — without a hard collision. The test particle experiences macroscopic electric and magnetic fields which give its trajectory a nonlinear kick. For example, a horizontally displaced proton passing through a round Gaussian bunch of size  $\sigma$  receives an angular kick

$$\Delta X' = -\frac{4\pi\xi}{\beta} \frac{2\sigma^2}{X} \left[ 1 - \exp\left(\frac{-X^2}{2\sigma^2}\right) \right] \quad [18]$$

where  $\xi$ , the “tune shift parameter,” is proportional to the transverse charge density in the bunch. The strength of the kick drops off like  $1/X$  at large displacements, unlike the polynomial behavior of magnetic kicks, since now the nonlinear field source is localised at the center of the beam pipe. Small amplitude trajectories receive kicks which are linear in displacement, as in a quadrupole, and are shifted in tune by  $\xi$  — hence the name, tune shift parameter. At large amplitudes the tune shift approaches zero, and the situation is usually stable, again in contrast to the magnetic case. Beam-beam resonances are strongest at intermediate amplitudes of a few sigma.

The maximum operational tune shift parameter is of order 0.02 per collision in electron rings, and of order 0.004 per collision in proton rings. This order of magnitude difference is largely due to the difference in transverse beam shape (electron beams are flat, proton beams are round, both are bigaussian) and to the fact that electrons produce a lot of synchrotron radiation, leading indirectly to a stabilising damping of the transverse motion. The SSC will be the first proton storage ring in which synchrotron radiation is significant, with a damping time of less than one day — electron ring damping times are typically measured in milliseconds. Somewhat different theoretical models are used to successfully explain the beam-beam limits in the two kinds of ring[27–31]. Good quantitative agreement between theory, simulation, and observation is only obtained in the proton case when tune modulation affects are taken into account[32–36]. The subject of tune modulation is returned to below.

Contemporary colliders store only a few — less than ten — bunches per beam, with particle and antiparticle beams counter-rotating in the same vacuum chamber. However, the frequency of collision decreases as the machines get larger, leading to a decrease in luminosity, unless there is an increase in the number of bunches or the charge per bunch. Both of these solutions come into violent conflict with the beam-beam limit, loosely defined as the maximum allowable tune shift per turn (not per collision). The SSC resolves this dilemma, and the associated problem of producing copious numbers of antiprotons, by filling two vertically separated storage rings with thousands of bunches of protons, longitudinally spaced by about 5 metres. Collisions between counter-rotating bunches are only allowed where they are useful. Consequently, the beam-beam effect is not expected to be critical in the SSC, although its presence will be noticed.

#### Radio Frequency Cavities

So far, the longitudinal motion of a test particle relative to the center of its own bunch has been ignored. Only transverse motion has been considered, although sometimes the test particle has had a constant off energy parameter  $\delta$ , and a displaced closed orbit. For example, a closed orbit trajectory with a large  $\delta$  of  $10^{-3}$  at a place with a typical dispersion function  $\eta$  of 3 metres is displaced outwards by 3 millimetres, and its single turn path length is about 2 centimetres longer than the design orbit. At the end of each turn a particle following this trajectory lags farther and farther behind the center of its bunch — if the speed of the particle is independent of its energy, a reasonable assumption in the relativistic limit. What, then, keeps a bunch of particles together? The answer is, a small number of short radio frequency cavities, each applying a longitudinal voltage which depends on the test particles longitudinal displacement from the center of its bunch. For the sake of simplicity, suppose that there is only one cavity, with a typical wavelength of about one metre. A nominal particle passes through this cavity when the field is zero, but a particle that arrives late loses energy, and an early particle gains energy.

So, the energy displacement  $\delta$  is not constant, but oscillates, with a typical period of hundreds of turns in proton storage rings, and tens of turns in electron storage rings. As is shown below, this situation appears at first sight to be analogous to the simple gravity pendulum. However, there is a crucial difference — the radio frequency restoring force is not applied continuously, like gravity, but is only applied as an impulse, once per turn of the

accelerator. That is, the gravity pendulum is a differential system, while longitudinal motion in an accelerator is a difference system. Difference systems like this which are analogous to the gravity pendulum are described by the “standard map,” which is so named because of its universal importance and frequent occurrence in many different nonlinear manifestations.

Even though nonlinear longitudinal motion does not limit the performance of any accelerator, the standard map is pedagogically well worth studying. Most resonant situations, including the most complex, can be reduced to a standard map by appropriate coordinate transformations (at least in principle). Equivalently, the standard map demonstrates many of the properties of more complex situations, such as chaos, the change of tune with amplitude, and the useful limits of a Hamiltonian description. For these reasons, longitudinal motion is the first nonlinear topic discussed here in detail.

#### LONGITUDINAL MOTION — THE STANDARD MAP

Suppose that a test particle circulates around a storage ring containing one radio frequency cavity. If the azimuthal reference point at which a Poincare surface of section is to be constructed is just before the cavity, then one turn consists of i) passage through the cavity, followed by ii) traversal of the rest of the machine. Although the RF cavity is typically several wavelengths long, it is reasonable to approximate it as an infinitesimally short impulse by integrating the electric field that the particle experiences into a single voltage. So, if the particle trails behind the center of its bunch by a positive distance of  $\Delta s$  when it passes through the cavity, its off energy parameter on turn  $t+1$  is related to that on turn  $t$  by

$$\delta_{t+1} = \delta_t - \frac{V_{RF}}{E_0} \sin(\theta_t) \quad [19]$$

where the RF phase angle

$$\theta_t = 2\pi \frac{\Delta s_t}{\lambda_{RF}} \quad [20]$$

is a natural longitudinal coordinate. The total path length during one turn varies with the energy according to

$$C = C_0 + 2\pi \langle \eta \rangle \delta \quad [21]$$

where  $\langle \eta \rangle$  is the average dispersion function in the bending dipoles. The additional term modifies  $\Delta s$  and  $\theta$ ,

$$\theta_{t+1} = \theta_t + \frac{(2\pi)^2 \langle \eta \rangle}{\lambda_{RF}} \delta_{t+1} \quad [22]$$

Equations [20] and [22], taken together, constitute the one turn map for longitudinal motion. Notice that the right hand side of [22] includes terms with both subscripts  $t$  and  $t+1$ .

It is now convenient to make a coordinate transformation, whose physical meaning will soon become apparent. Replacing  $\theta$ ,  $\delta$  and the physical parameters in [20] and [22] with the quantities

$$q = \theta, \quad p = 2\pi \left( \frac{\langle \eta \rangle}{\lambda_{RF}} \frac{E_0}{V_{RF}} \right)^{1/2} \delta, \quad \Delta T = 2\pi \left( \frac{\langle \eta \rangle}{\lambda_{RF}} \frac{V_{RF}}{E_0} \right)^{1/2} \quad [23]$$

the map becomes

$$p_{t+1} = p_t - \Delta T \sin(q_t) \quad [24]$$

$$q_{t+1} = q_t + \Delta T p_{t+1}$$

This is the standard map. If  $q$  is always small, it has an approximate linear solution of

$$q_t = q_0 \cos(2\pi Q_S t) \quad [25]$$

where the small oscillation tune,  $Q_S$ , is called the synchrotron tune in the particular case of longitudinal oscillations. It is given by

$$\cos(2\pi Q_S) = 1 - \frac{\Delta T^2}{2} \quad [26]$$

which shows that even small amplitude motion is unstable under the standard map if  $\Delta T$  is greater than 2. In electron storage rings  $Q_S$  is typically between 0.01 and 0.1, while in proton storage rings it is typically an order of magnitude smaller.

The physical meaning of the coordinates  $q$  and  $p$ , and the parameter  $\Delta T$ , is made clear by taking the standard map to be the numerical representation of a rigid pendulum of unit length, with the acceleration due to gravity set equal to one. In this case  $q$  corresponds to the angle the pendulum makes with vertical,  $p$  corresponds to the angular velocity of the pendulum  $dq/dt$ , and  $\Delta T$  corresponds to the integration time step size. Since the continuous time  $T$  is given in terms of the discrete time  $t$  by

$$T = t \Delta T \quad [27]$$

and since  $2\pi Q_S = \Delta T$  for small time steps, the small angle motion of the pendulum is simply

$$q(T) = q_0 \cos(T) \quad [28]$$

It is not surprising that the time step must be much less than the natural period of the system — much less than one — for such a discrete representation of a differential system to be accurate. What is surprising, perhaps, is that the dynamics of analogous differential and difference systems are qualitatively different.

The most compact way to describe the differential pendulum system is by means of a Hamiltonian,

$$H = \frac{1}{2} p^2 - \cos(q) \quad [29]$$

which, by definition, is shorthand for the equations of motion

$$\frac{dq}{dT} = \frac{\partial H}{\partial p} \quad [30]$$

$$\frac{dp}{dT} = -\frac{\partial H}{\partial q}$$

Trajectories of the pendulum system follow contours of the Hamiltonian function, because  $H$  is explicitly conserved, since

$$\frac{dH}{dT} = \frac{\partial H}{\partial p} \frac{dp}{dT} + \frac{\partial H}{\partial q} \frac{dq}{dT} = 0 \quad [31]$$

by substitution of the equations of motion[30]. The rate of progress along a contour depends only on the local slope of the Hamiltonian function. These two properties make it easy to picture the behavior of a one dimensional system, if only a Hamiltonian can be constructed from the equations of motion.

Figure 3a shows the contours of the pendulum Hamiltonian. Equivalently, it shows the Poincare surface of section of the longitudinal motion of particles in a storage ring, in the limit that  $Q_S$  goes to zero. A trajectory near the center of the plot exhibits stable, limited, oscillations — the pendulum has a maximum absolute angle, or, equivalently, the particle is trapped inside a single RF “bucket.” A trajectory near the top or bottom will eventually reach all values of the coordinate  $q$  — the pendulum is rotating continuously, or the particle is not associated with any particular bunch. The boundary between these qualitatively different kinds of motion, trapped and untrapped, is called the “separatrix.” It takes an infinite amount of time to move once around the separatrix, since the slope of  $H$  is zero at the “unstable fixed points” where the pendulum is inverted and motionless. Equivalently, the longitudinal tune of a particle shifts from  $Q_S$  at the centre of the RF bucket, to zero at its edges.

From the pendulum point of view, the standard map is merely an approximation of the differential equations of motion, via

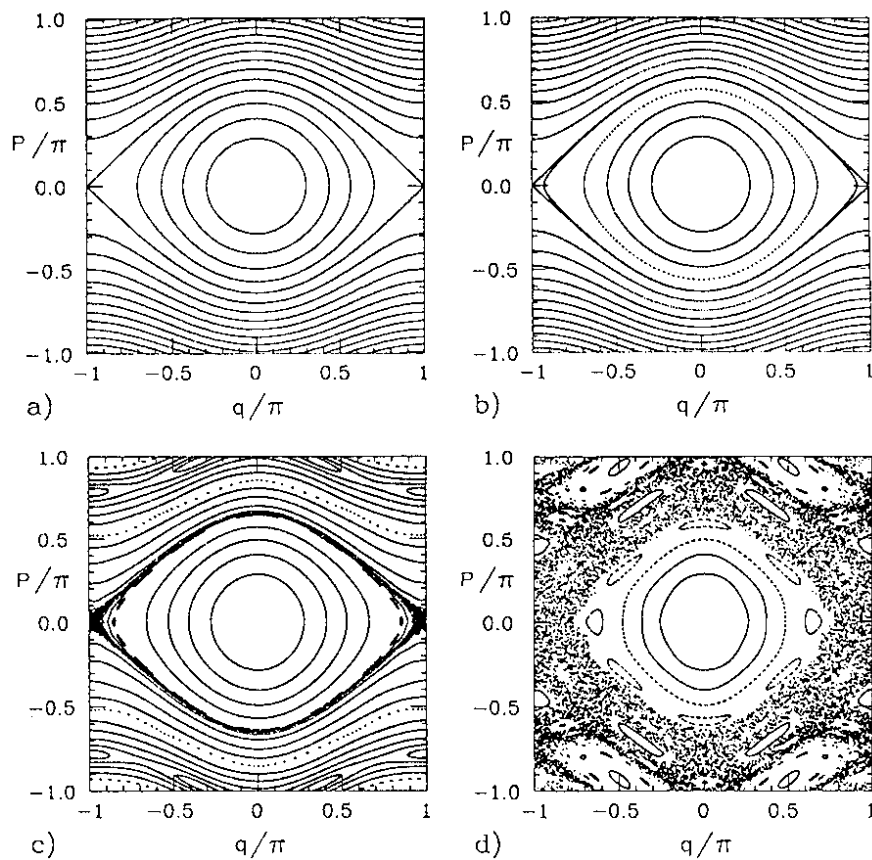


Figure 3. Standard map trajectories, with four different synchrotron tunes,  $Q_S$ , corresponding to different integration time steps,  $\Delta T$ . a) Contours of the Hamiltonian  $H = (P^2/2) p^2 - \cos(q)$ , representing the differential pendulum. b)  $Q_S = 0.06$ . Almost indistinguishable from a), with no sign of chaos, even close to the “separatrix.” c)  $Q_S = 0.12$ . A narrow chaotic region appears near the “separatrix,” and some secondary islands appear. d)  $Q_S = 0.18$ . Most of phase space is chaotic, surrounding complex island structures.

$$\Delta q = \frac{\partial H}{\partial p} \Delta T \quad [32]$$

$$\Delta p = -\frac{\partial H}{\partial q} \Delta T$$

However, from the RF cavity point of view, the Hamiltonian representation is merely an approximation of the difference equations of motion. It depends upon the physical case in hand whether a continuous or discrete representation is more appropriate. Figure 3b shows how trajectories with a small value of  $Q_S = 0.06$  respond to the standard map almost exactly as if the system was continuous. (To keep the plot symmetric, the azimuthal reference point has been moved to the center of the RF cavity, instead of just before it). One dot is drawn per iteration of the map, for many iterations of several different trajectories. Except for one trajectory, these dots appear to form continuous lines — “KAM surfaces”[37–40] — looking like the contours of the continuous Hamiltonian.

In a region of phase space which is regular, where trajectories form KAM contours, two infinitesimally close neighboring trajectories diverge linearly with time. When  $Q_S$  is increased to 0.12 and 0.18, in Figures 3c and 3d, chaotic trajectories appear with scattered dots. In chaotic regions of phase space, infinitesimally close neighboring trajectories diverge exponentially with time. Chaos first becomes visible in Figure 3c near where the separatrix used to be — there are no separatrices in difference systems — in a region which is bounded by KAM surfaces. Most of phase space is chaotic in Figure 3d, and it is hard to say whether chaotic regions bound regular regions, or vice versa.

Both Figures 3c and 3d also show secondary resonance island structure in addition to the main island at the center of the plot. For example, there is a chain of 16 small islands near the (now non-existent) main separatrix in Figure 3c. Comparatively large islands are also visible near the top and bottom of the figure, in the “untrapped” part of phase space. These are resonances on the backs of resonances, an example of the kind of recursive structure which is often associated with chaotic behavior. It is not too surprising to learn that, if motion around these sub-resonances is examined in detail, then it, too, can be described in terms of the standard map. And so on, ad infinitum.

The fundamental difference between the differential pendulum and the difference pendulum is that the restoring force is time independent in the first “autonomous” case, and is time independent in the second, “non-autonomous” case. This is conveniently illustrated by rewriting the standard map as a single, second order, differential equation in  $q$

$$\frac{d^2 q}{dT^2} = - \sum_{n=-\infty}^{\infty} \delta(T-n\Delta T) \Delta T \sin(q) \quad [33]$$

where the delta function  $\delta(\ )$  is not to be confused with the off energy parameter. Neighboring trajectories in one dimensional autonomous systems show only linear divergence, while non-autonomous systems can also show exponential divergence. Systems of two or more dimensions can always show exponential divergence — chaos.

#### SEXTUPOLES — THE HENON MAP

One of the earliest dynamicists to attempt a general numerical study of nonlinear maps was Henon, an astrophysicist[41]. He found that the map which now bears his name “exhibits all the typical properties of more complicated mappings and dynamical systems.” This one-dimensional map is directly relevant to accelerator physics, as it describes an accelerator in which there is a single nonlinearity, a thin sextupole, of unit strength. In normalised coordinates the motion around the linear part of the machine amounts simply to a

coordinate rotation, so if the reference point for the Poincare surface of section is just before the sextupole, then the map from turn  $t$  to turn  $t+1$  is just

$$\begin{pmatrix} x_{t+1} \\ x'_{t+1} \end{pmatrix} = \begin{pmatrix} C & S \\ -S & C \end{pmatrix} \begin{pmatrix} x_t \\ x'_t + x_t^2 \end{pmatrix} \quad [34]$$

where  $C = \cos(2\pi Q_0)$  and  $S = \sin(2\pi Q_0)$ , in which  $Q_0$  is the tune of a small amplitude trajectory. Figures 4a through 4d are taken almost directly from a paper by Henon, showing surface of section plots of several trajectories for four values of the control parameter  $Q_0$ , near to  $1/3$ ,  $1/4$ ,  $1/5$  and  $1/6$ .

Four different kinds of trajectories can be loosely distinguished. Regular non-resonant trajectories are found close to the origin of each of the figures. The trajectories are regular, but become distorted away from circles at moderate and large amplitudes. As discussed both above and below, the deviation from circularity is conveniently measured by the smear.

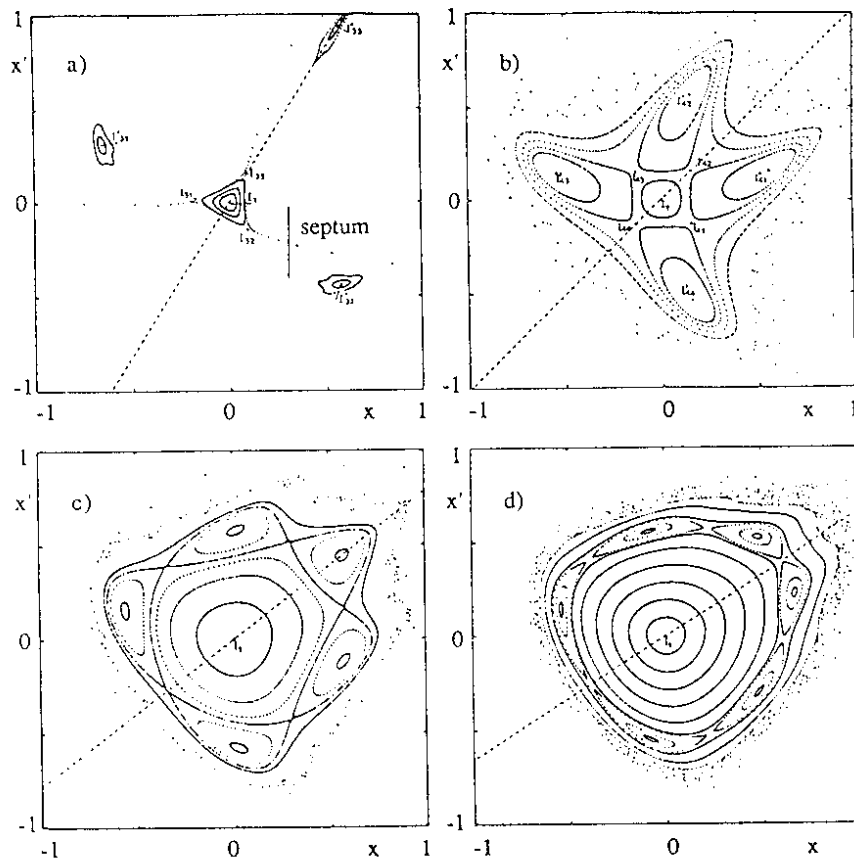


Figure 4. Trajectories obtained by Henon[41] from iterating his map with different base tunes,  $Q_0$ . When  $Q_0 \approx 1/n$ ,  $n$  resonance islands appear. a)  $Q_0 = 0.324 \approx 1/3$ . The stable triangle and the divergent arms are well described by first order theory, but the outlying islands are not. b)  $Q_0 = 0.2516 \approx 1/4$ . Four big islands at a small amplitude, with  $Q_0$  very close to  $1/4$ . c)  $Q_0 = 0.211 \approx 1/5$ . Five islands, surrounded by a stable KAM contour, and then chaos. d)  $Q_0 = 0.185 \approx 1/6$ . The six islands are almost rotationally symmetric - they resemble each other and the standard map structure.

Under normal stable operation of a storage ring the beam fills only the small smear region. The deviations from circularity increase as the amplitude gets larger, until the motion breaks up into regular resonant trajectories, forming a chain of resonance islands. The number of islands corresponds to the denominator of the rational fraction nearest to  $Q_0$ . Chaotic trajectories occur at the largest amplitudes in the figures (except in Figure 4a where chaotic points have been removed for the sake of clarity). While some of these trajectories are bounded, as in the case of the standard map, some appear to diverge to infinity. This is because the  $x^2$  nonlinear term in the Henon map is unbounded, unlike the  $\sin(q)$  term in the standard map.

Rapidly divergent regular trajectories can be seen in figure 4a, in the form of three arms of widely spaced dots whose amplitude increases rapidly from turn to turn. This behavior is very useful in the controlled extraction of particles from a storage ring, as illustrated by the inclusion of a “septum” in the figure. The septum is a current or charge carrying metallic membrane, arranged so that there is no magnetic or electric field on the inside, while on the outside a particle is deflected into an extraction line. For the extraction efficiency to be high, the septum must be thin compared to the amplitude increase in three successive turns. More and more particles are squeezed out of the stable triangle at the center of the beam pipe by gradually moving the base tune  $Q_0$  closer and closer to  $1/3$ . Despite appearances, these trajectories are really only regular resonant trajectories, since, given enough time and an enormous vacuum chamber, a particle following one of these trajectories would eventually return to the small amplitude region.

#### Smear, and the First Order Discrete Hamiltonian, $H_1$

It is relatively straightforward to solve the equations of motion for the distortions which perturb the circular trajectories near the center of the plots — at least to first order in the sextupole strength  $g$ , where

$$\Delta x' = gx^2 \quad [35]$$

First, though, it is convenient to introduce “action-angle” coordinates,  $J$  and  $\phi$ , where

$$\begin{pmatrix} x \\ x' \end{pmatrix} = \begin{pmatrix} (2J)^{1/2} \sin(\phi) \\ (2J)^{1/2} \cos(\phi) \end{pmatrix} \quad [36]$$

That is, the action  $J$  behaves very much like the betatron amplitude, while  $\phi$  is explicitly the betatron phase of the trajectory under study. It is easy to show that the motion from turn  $t$  to  $t+1$  is described to first order in  $g$  by

$$\begin{pmatrix} J \\ \phi \end{pmatrix}_{t+1} = \begin{pmatrix} J \\ \phi \end{pmatrix}_t + \begin{pmatrix} -\frac{\partial H_1}{\partial \phi} \\ \frac{\partial H_1}{\partial J} \end{pmatrix}_t \quad [37]$$

where the one turn “discrete” Hamiltonian  $H_1$  is given by

$$H_1 = 2\pi Q_0 J + \frac{g}{3\sqrt{2}} J^{3/2} [ \sin 3(\psi + \phi) - 3 \sin (\psi + \phi) ] \quad [38]$$

in which  $\psi$  is the constant phase of the single sextupole, relative to the reference point. The first term in this discrete Hamiltonian corresponds to the linear phase advance of  $2\pi Q_0$ , as expected.

Not one, but sixteen sextupoles dominate the nonlinear behavior of the Tevatron in the E778 experiment. More generally, then, the Hamiltonian is written as

$$H_1 = 2\pi Q_0 J + \sum_{\{ik\}} V_{ik} J^{i/2} \sin(k\phi + \phi_{ik}) \quad [39]$$

where the sum is over  $ik$  pairs

$$\{ik\} = \{33, 31\} \quad [40]$$

The constants  $V_{ik}$  and  $\phi_{ik}$  are obtained from a vector sum of the terms proportional to  $g$  in equation [38], over all sextupoles. Equation [40] is not exactly correct, but only describes the motion correctly to first order in sextupole strength, since higher order terms have been ignored. This first order result for  $H_1$ , and the results which follow, are easily generalised further. For example, if octupole nonlinearities are also present, the set  $\{ik\}$  is extended to become  $\{30,31,44,42,40\}$ . Or, if two dimensional motion in the presence of sextupoles is to be described, it is expanded to  $\{ijkl\} = \{3030,3010,1210,1212,121-2\}$ , where  $j/2$  is the exponent of the vertical action, and  $l$  is the coefficient of the vertical betatron phase. What is hard is to extend the description to higher order in nonlinear strengths.

The action is a smooth function of the phase,  $J(\phi)$ , if the motion is regular and non-resonant. Substituting the lowest order solution of phase motion

$$\phi_t = 2\pi Q_0 t + \phi_0 \quad [41]$$

into the difference equation of motion for  $J$  in [37] gives

$$J(\phi + 2\pi Q_0) - J(\phi) = - \frac{\partial H_1}{\partial \phi} \quad [42]$$

Using the Hamiltonian in equation [39] gives, for perturbations small compared to  $J_0$ ,

$$J(\phi) = J_0 - \sum_{\{ik\}} \frac{k V_{ik}}{2 \sin(k\pi Q_0)} J_0^{i/2} \sin(k\phi + \phi_{ik} + k\pi Q_0) \quad [43]$$

A resonance denominator appears here, for the first time — if the base tune  $Q_0$  is near an integer or an integer divided by three, then one of the terms in the sum becomes large and can destroy the original assumption that the perturbation is small. The  $k=3$  term causes the characteristic triangular shape seen in Figure 4. In order to describe the 4, 5, or 6 fold structure that leads up to the resonance islands in Figure 4, it is clearly necessary to include higher order terms in the discrete Hamiltonian.

Substituting the phase motion given in [41] into [43] gives the action as a function of turn number,

$$J_t = \langle J \rangle - \sum_{\{ik\}} \frac{k V_{ik}}{2 \sin(k\pi Q_0)} J_0^{i/2} \sin(2\pi k Q_0 t + \phi_{0ik}) \quad [44]$$

where  $\langle J \rangle = J_0$  is the average action, and  $\phi_{0ik} = k\phi_0 + \phi_{ik} + k\pi Q_0$  is a constant phase. In terms of amplitude rather than action, the motion is

$$a_t = \langle a \rangle - \sum_{\{ik\}} \frac{k V_{ik}}{2^{i/2+1} \sin(k\pi Q_0)} a_0^{i-1} \sin(2\pi k Q_0 t + \phi_{0ik}) \quad [45]$$

According to the definition given in equation [14], the one dimensional smear is

$$S = \langle a \rangle \sqrt{\frac{3^2 V_{33}^2}{2^6 \sin^2(3\pi Q_0)} + \frac{V_{31}^2}{2^6 \sin^2(\pi Q_0)}} \quad [46]$$

showing that the smear due to sextupoles increases linearly with amplitude, for small amplitudes. The displacement  $x(t)$  at the reference point, which can be detected by a beam position monitor (BPM), is

$$x_t = a_t \sin(2\pi Q_0 t + \phi_0) \quad [47]$$

$$= \langle a \rangle \sin(2\pi Q_0 t + \phi_0) - \sum_{\{ik\}} \frac{k V_{ik}}{2^{i/2+2} \sin(k\pi Q_0)} a_0^{i-1} [\cos(2\pi(k-1)Q_0 t + \phi_{0ik} - \phi_0) - \cos(2\pi(k+1)Q_0 t + \phi_{0ik} + \phi_0)] \quad [48]$$

Since  $k = 1$  or  $3$  for sextupoles, Fourier analysis of a turn-by-turn BPM signal reveals harmonics at  $2Q_0$  and  $4Q_0$ , in addition to the fundamental signal.

#### Experimental observation of smear

Two analyses are readily available for measuring smear from turn-by-turn position data, corresponding to treatment in the frequency domain and in the time domain. While E778 has so far concentrated on time domain measurements of one-dimensional motion, frequency domain measurements will be essential in the imminent studies of two dimensional oscillations. Both analysis techniques are complicated by the finite size of the beam, as will be seen.

The basic experiment is very simple — kick the beam horizontally on turn 0, inducing an oscillation of amplitude  $a_{kick}$ , and observe the ensuing oscillations for at least a hundred turns on two neighboring BPMs. If the two signals on a given turn  $t$  are  $x_1(t)$  and  $x_2(t)$ , then the amplitude  $a_t$  on that turn is given by

$$a_t^2 = c_{11} x_1^2 + c_{12} x_1 x_2 + c_{22} x_2^2 \quad [49]$$

where the coefficients  $c_{11}$ ,  $c_{12}$ , and  $c_{22}$  depend on the beta values at the two BPMs,  $\beta_1$  and  $\beta_2$ , and on the betatron phase advance  $\Delta\phi_{12}$  between them. For example, if  $\beta_1 = \beta_2$  and  $\Delta\phi_{12} = 90$  degrees, then  $c_{11} = c_{22} = 1$ , and  $c_{12} = 0$ . Having established the time sequence  $a_t$  for a sufficient number of turns, the smear is obtained directly from equation [14]. Practical problems associated with non-zero closed orbit offsets, and  $\beta$  and  $\phi$  errors, are easily overcome.

The data taken and processed in this way in Figure 5 show that, instead of the amplitude being approximately constant (within smear variations), there is an initial gaussian decay of the signal. This decay is due to the finite size of the beam, which implies a distribution of initial amplitudes in a typical range  $a_{kick} \pm \sigma$ , where  $\sigma$  is the gaussian beam size. The spread in amplitudes leads to a spread in tunes across the beam, of size  $\Delta Q = \sigma(dQ/da)|_{a_{kick}}$ , causing the signal to decohere with a gaussian time constant of  $1/\Delta Q$  turns. It is straightforward to compensate for the decoherence in calculating the smear during one dimensional motion.

The equivalent frequency domain measurement consists of Fourier analysing the signal from either one or both of the BPMs, as described theoretically in [47], and then reconstructing the values of  $V_{33}$  and  $V_{31}$ , ready for substitution into [46] for evaluation of the smear. Using only one BPM leads to some problems in reconstructing the  $V$  values, since the response at  $2Q_0$ , for example, depends on  $V_{33}$ ,  $V_{31}$ ,  $\phi_{033}$ , and  $\phi_{031}$ . Information from two BPMs is needed to derive the phases  $\phi_{033}$ , and  $\phi_{031}$ , or to construct the amplitude time series for subsequent Fourier analysis. Finite beam size also causes

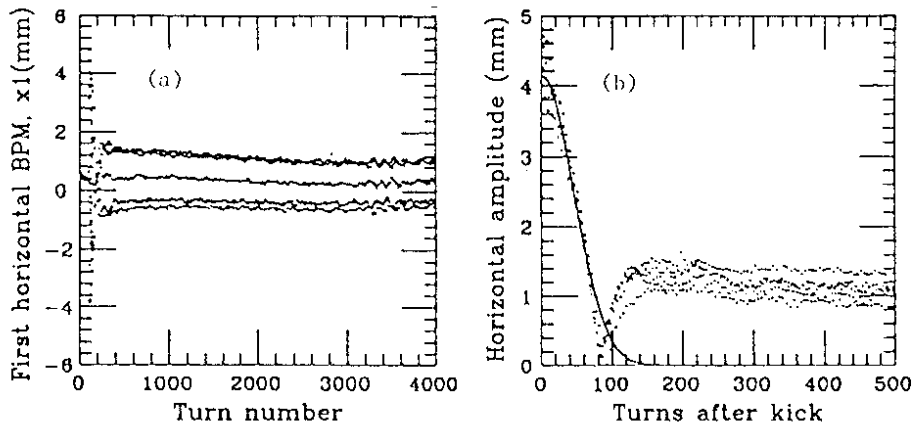


Figure 5. Typical data from the E778 experiment, showing both Gaussian decoherence and a persistent signal. a) Raw turn-by-turn data taken by one of the beam position monitors, over 4,000 turns. The signal strength initially drops very rapidly after a transverse deflection of about 4 millimetres, finally leaving five persistent signal lines with a very slow decay rate. b) The reconstructed amplitude over the first 500 turns, showing that the initial decoherence is well fitted by the solid line Gaussian. About 30% of the beam is trapped in a resonance island at an amplitude of about 4 millimetres.

problems in the frequency domain, by broadening peaks which would otherwise be sharp. So long as the peaks do not overlap, it is relatively straightforward to derive the single particle equivalent amplitudes and phases.

#### Five Islands — the Single Resonance Hamiltonian, $H_5$

The simple solution to the equations of motion given above, [41] and [43], breaks down when the motion is resonant, or nearly resonant. For example, suppose that the coefficient set  $\{ik\}$  in equation [43] is somehow extended to include  $k=5$  (and hence  $i \geq 5$ ) in trying to describe the phase space distortions close to the five-fold island structure seen in Figure 4c. As the tune  $Q_0$  approaches  $1/5$ , the shrinking resonance denominator  $\sin(5\pi Q_0)$  eventually leads to a violation of the original assumption of small distortions — and predicts infinite distortions when  $Q_0=1/5$ , on resonance. The source of this error lies in assuming the simple phase advance per turn given by equation [43]. When a trajectory is trapped in a resonance island, the solution is better given by an expression like [13]. The trapped and untrapped approximate solutions for the phase illustrate the topological difference between resonant and non-resonant motion. Given enough time, the phase of a non-resonant trajectory will come arbitrarily close to any given phase. In contrast, the phase of a resonant trajectory has only a limited range of possible values.

There are two important experimental questions to ask about a resonance. First, how wide is it? That is, what amplitude or action range does it span. Second, what is the tune  $Q_1$  at the center of the islands? These questions are answered theoretically by concentrating on a single resonance denominator, say five, and by developing a Hamiltonian description of the five-turn motion. That is, whereas so far  $t$  has been implicitly integer, soon  $t$  will be an integer which is exactly divisible by five. As a starting point, assume that the tune  $Q_0$  is close to  $2/5$ , as in the resonance investigations of the E778 experiment, and assume that the one turn Hamiltonian  $H_1$  has somehow been developed to include a complete set of coefficients with  $i,k \leq 5$ , specifically  $\{ik\} = \{33,31,44,42,40,55,53,51\}$ .

It can be shown that only terms with  $k=0$  and  $k=5$  survive when  $H_1$  is averaged over 5 turns, so that the “single resonance Hamiltonian” becomes

$$H_5 = 2\pi \left(Q_0 - \frac{2}{5}\right) J + V_{40} J^2 + V_{55} J^{5/2} \sin(5\phi + \phi_{55}) \quad [50]$$

This is just shorthand for the five-turn difference equations of motion

$$\begin{pmatrix} J \\ \phi \end{pmatrix}_{t+5} = \begin{pmatrix} J \\ \phi \end{pmatrix}_t + 5 \begin{pmatrix} -\frac{\partial H_5}{\partial \phi} \\ \frac{\partial H_5}{\partial J} \end{pmatrix}_t \quad [51]$$

by analogy with the single turn equations of motion, equation [37]. The meaning of the three terms in  $H_5$  becomes clear when the partial differentiations in [51] are performed. For example, the first term corresponds to a five turn phase advance of  $5 \cdot 2\pi (Q_0 - 2/5)$ , independent of the action. Subtraction of  $2/5$  from  $Q_0$  is justified by noting that it leads to an inconsequential subtraction of  $4\pi$  from the five turn phase advance. The subtraction is motivated by making the coefficient of  $J$  a small number. Next, differentiation of  $V_{40} J^2$  with respect to  $J$  leads to a five turn phase advance of  $10 V_{40} J$ , linearly proportional to the action.

Temporarily ignoring the third term, there is an octupolar tune shift with action or amplitude, given by

$$Q(J) = Q_0 + \frac{V_{40}}{\pi} J = Q_0 + \frac{V_{40}}{2\pi} a^2 \quad [52]$$

The action  $J_1$  at which  $Q(J_1) = 2/5$  identifies where the resonance is found. Before examining the behavior of the term in  $V_{55}$ , it is convenient to make a coordinate transformation and rewrite  $H_5$  as an expansion around  $J_1$ ,

$$H_5 = \frac{1}{2} U I^2 - V \cos(5\phi) \quad [53]$$

where

$$I = J - J_1, \quad U = 2 V_{40}, \quad V = V_{55} J_1^{5/2} \quad [54]$$

and the value of  $\phi_{55}$  has been conveniently chosen.

Substitution of this Hamiltonian into the equations of motion [51] (with  $J$  replaced by  $I$ ) shows that  $(I, \phi) = (0, 0)$  is a fixed point — a trajectory launched there is stationary. This is in marked contrast with the usual single turn motion, in which a trajectory always advances by a large phase of about  $2\pi Q_0$ , even in the absence of nonlinearities. In some region close enough to  $I = 0$ , then,  $H_5$  may be considered as representing differential equations of motion, continuous in  $t$ , which agree well with the difference motion whenever  $t$  is an integer multiple of five. In this approximation

$$\begin{pmatrix} \frac{dI}{dt} \\ \frac{d\phi}{dt} \end{pmatrix} = \begin{pmatrix} -\frac{\partial H_5}{\partial \phi} \\ \frac{\partial H_5}{\partial I} \end{pmatrix} = \begin{pmatrix} -5V \sin(5\phi) \\ U I \end{pmatrix} \quad [55]$$

which, except for factors of 5, is the familiar case of the pendulum. For small angles,  $\delta\phi \ll 1/5$ , the solution of these equations is just

$$\begin{pmatrix} I \\ \phi \end{pmatrix} = \begin{pmatrix} 5 \left(\frac{V}{U}\right)^{1/2} \sin(2\pi Q_I t) \\ \cos(2\pi Q_I t) \end{pmatrix} \quad [56]$$

where it may be assumed that  $V$  and  $U$  are both positive. The island tune is given by

$$Q_I = \frac{5}{2\pi} (UV)^{1/2} \quad [57]$$

This answers the second of the two key questions about the resonance. Now return to the first question — what is the resonance width?

The approximate representation of the motion by differential equations of motion is valid “close enough” to the center of the islands, and for island tunes  $Q_I$  much less than one. A trajectory in this region follows contours of constant  $H_5$  very closely. The shape of the Hamiltonian hillside is a parabolic valley along the  $I$ -axis, with a modulation along the  $\phi$ -axis caused by the  $\cos(5\phi)$  term which leads to five local minima separated by five saddle points, corresponding to five stable and five unstable fixed points.

The amplitude width of the islands is estimated by assuming that trajectories at least as far as the separatrix follow  $H_5$  contours. (This is explicitly wrong very close to the separatrix, which does not even exist in the difference system.) Since trajectories follow contours of  $H_5$ , and since the saddle point (unstable fixed point) is on the boundary between resonant and non-resonant motion, the height of the saddle point,  $H_5(0, 2\pi/10)$ , is the same as the height  $H_5(I_W, 0)$ , where  $I_W$  is the island half width. This gives

$$I_W = 2 \left(\frac{V}{U}\right)^{1/2} \quad [58]$$

This is readily converted to an amplitude width by dividing by  $a_I$ , the resonance amplitude.

#### Experimental Resonance Observation

In an experiment, the resonance amplitude  $a_I$  is adjusted by changing  $Q_0$ , so long as it remains inside the dynamic aperture. This has a strong effect on both  $Q_I$  and  $a_W$ , especially for high order resonances, since  $Q_I$  goes like  $a_I^{n/2}$ , and  $a_W$  goes like  $a_I^{(n-2)/2}$ , where  $n$  is the order of the resonance. At first sight measurements of resonances appear to be overconstrained, since there are two parameters in the theoretical model,  $U$  and  $V$ , while there are three experimental observables,  $d^2Q/da^2$ ,  $Q_I$  and  $a_W$ , which are related to each other by equations [52], [57], and [58]. This would provide a stringent test of the model. Unfortunately, life is not that simple, again because of the finite beam size. In practice,  $d^2Q/da^2$  is easily measured to about 10%, but the determination of  $Q_I$  and  $a_W$  to this accuracy is more difficult.

Figure 5 illustrates typical data obtained by kicking the gaussian beam into a phase space position which partially overlaps fifth order islands. At first the signal undergoes the usual gaussian decoherence. However, there is also a “persistent signal,” which has a very small decay rate — it is typically observed for tens of seconds, or millions of turns. This signal is due to particles which do not decohere because they are phase locked within the bounds of a resonance island. If the base tune  $Q_0$  is adjusted to maximise the persistent signal strength, when  $a_{kick} \approx a_I$ , the persistent amplitude leads directly to the resonance width  $a_W$ , through

$$\frac{a_{persistent}}{a_{kick}} = G \frac{a_W}{\sigma} \quad [59]$$

where  $G$  is a geometrical factor close to unity which is calculated by numerical simulation[2,3,9]. The beam size  $\sigma$  is assumed to be well known, although in practice it

fluctuates from shot to shot. Once measurements of  $a_w$  have been made at several values of  $a_{kick}$ , the set of data pairs  $(Q_0, a_{kick})$  are analysed to yield an accurate plot of tune versus amplitude.

Measurement of  $Q_I$  is not so straightforward. If the beam size is much smaller than the island size, then Fourier analysis of the time series  $\{\phi_t - 2\pi(2/5)t\}$  leads to a sharp peak at  $Q_I$ , if the phase amplitude  $\delta\phi$  in [13] is small. If the phase amplitude is large, then several peaks are seen, at harmonic multiples of a value of a fundamental tune which is smaller than the value  $Q_I$  at the center of the island. In practice the beam size is relatively large and Fourier analysis reveals a broad spectrum, due to the spread in  $Q_I$ . A better way to measure  $Q_I$  experimentally, independent of beam size, is by observing the response of a persistent signal to tune modulation.

### TUNE MODULATION

If a set of quadrupoles is perturbed by a small sinusoidal current, the tune of a small amplitude trajectory is modulated according to

$$Q_0 = Q_{00} + q \sin(2\pi Q_M t) \quad [60]$$

where  $q$  and  $Q_M$  are the tune modulation amplitude and tune. Power supply ripple like this is normally carefully avoided, especially in proton colliders, where any source of noise degrades the storage lifetime of the beam. (This in itself is a good reason for deliberately introducing tune modulation in a controlled experiment.) Noisy quadrupoles are particularly troublesome during the slow extraction of protons, when the smooth approach of the tune to a low order resonance is necessary to ensure a steady spill rate. Special fast quadrupoles are used during slow extraction in the Tevatron, responding to the difference between measured tune and requested tune, to compensate for such noise. It is these quadrupoles which E778 uses in its investigation of resonance behavior in the  $(q, Q_M)$  parameter space. As Figure 6 shows, the  $(q, Q_M)$  plane is rich in dynamical features. The dotted line in the figure shows the region accessible to the experiment, with maximum  $q$  and  $Q_M$  values of about 0.01.

Tune modulation is included in the resonance Hamiltonian near a fifth order resonance by adding a single term to equation [53], to give

$$H_5 = 2\pi q \sin(2\pi Q_M t) I + \frac{1}{2} U I^2 - V \cos(5\phi) \quad [61]$$

This Hamiltonian is still shorthand for two differential equations, not difference equations, because of the very small net motion in five turns. Unfortunately,  $H_5$  is now time dependent, and so is no longer conserved. The two first order equations of motion are now

$$\begin{pmatrix} \frac{dI}{dt} \\ \frac{d\phi}{dt} \end{pmatrix} = \begin{pmatrix} -5V \sin(5\phi) \\ 2\pi q \sin(2\pi Q_M t) + UI \end{pmatrix} \quad [62]$$

or, as a single second order differential equation in  $\phi$

$$\frac{d^2\phi}{dt^2} + (2\pi Q_I)^2 \frac{\sin(5\phi)}{5} = (2\pi)^2 q Q_M \cos(2\pi Q_M t) \quad [63]$$

This is physically analogous to the motion of a rigid pendulum, of small amplitude natural tune  $Q_I$ , which is driven by an external torque. (The factors of 5 could easily be removed by a scale change). Just as longitudinal motion was interesting because of its connection to the universally recurring standard map, the effect of tune modulation on accelerator resonances is interesting as a representation of the driven differential pendulum.

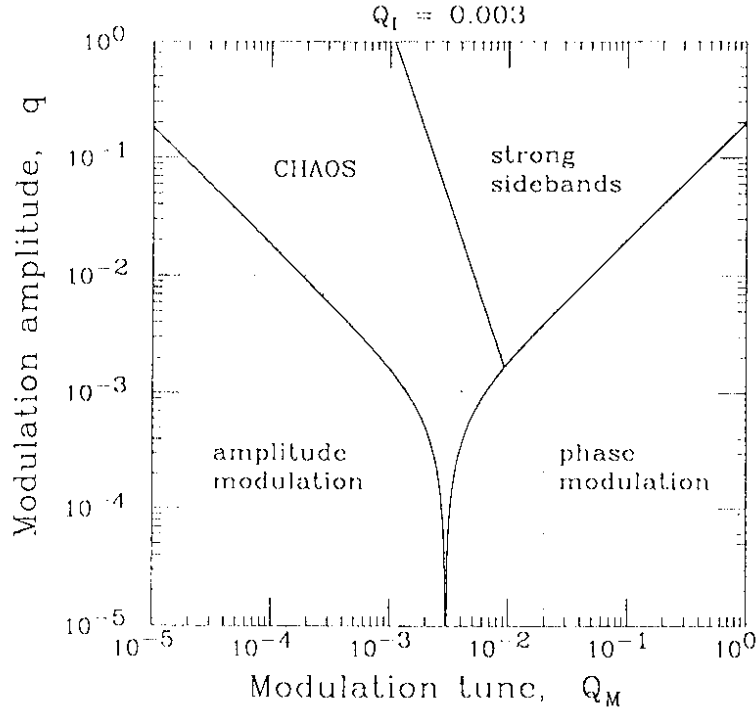


Figure 6. Dynamical behavior in different regions of the tune modulation parameter space  $(Q_M, q)$ , for a value of  $Q_I = 0.003$ . The dotted line shows the region accessible to the E778 experiment, extending beyond the resonance pole at  $Q_M = Q_I$  for this particular value of the island tune, which is relatively small.

If the motion is not chaotic, the general form of the solution for the phase of a trapped particle is a double Fourier series expansion in both the driving tune  $Q_M$ , and in a free oscillation tune, which is shifted below  $Q_I$  at moderate or large amplitudes. However, the experimental observable in E778 is the persistent signal picked up at a BPM, which depends on the average motion of the distribution of trapped particles. It seems reasonable to assume (but is only an approximation) that the center of charge motion which is detected is the same as that of a trajectory with no free oscillation amplitude. Hence we are mostly interested in a solution to the equation of motion which is a single Fourier expansion in the coherent driving tune,  $Q_M$ . There is a family of possible periodic solutions, labeled by the integer  $k$ ,

$$5\phi = k 2\pi (Q_M t) + \sum_{n=1}^{\infty} c_n \cos(n 2\pi Q_M t) \quad [64]$$

where the coefficients  $c_n$  are functions of  $q$ ,  $Q_M$ , and  $Q_I$ .

The first term in [64], linear in  $t$ , corresponds in the pendulum system to gaining or losing exactly  $k$  complete turns in one modulation period. In the accelerator system the linear term leads to the possibility of stable resonance islands at a family of sideband tunes, since

$$Q_{\text{solution}} = \frac{2}{5} + \frac{1}{2\pi} \left\langle \frac{d\phi}{dt} \right\rangle = \frac{2}{5} + k \frac{Q_M}{5} \quad [65]$$

Each sideband represents five resonance islands, with centers at an action  $I_k$  given by

$$Q(I_k) = \frac{2}{5} + \frac{UI_k}{2\pi} = Q_{\text{solution}} \quad [66]$$

so that

$$I_k = k \frac{2\pi Q_M}{5U} \quad [67]$$

The interesting question is whether the  $k$ -th solution is stable. If it is, then it should be possible to observe persistent signals at the corresponding sideband tune, by kicking a beam on top of one of the sideband islands.

Rigorous analytical results for the solutions exist only in the slow and fast modulation limits, when  $Q_M$  is much smaller or much larger than  $Q_I$ . For large amplitude oscillations in the intermediate region it is necessary to rely on iterative solutions and on simulations. The  $k=0$  solution in the small angle limit  $5|\phi| \ll 1$  is illuminating. It is given, for all values of  $Q_M$ , by

$$\phi = \frac{Q_M^2}{Q_I^2 - Q_M^2} \frac{q}{Q_M} \cos(2\pi Q_M t) \quad [68]$$

and

$$I = -\frac{Q_I^2}{Q_I^2 - Q_M^2} \frac{2\pi q}{U} \sin(2\pi Q_M t)$$

Both expressions include the same resonance denominator, but with different numerators. At constant  $q$ , the amplitude of the action oscillation goes to  $(2\pi q)/U$  for small  $Q_M$  and to zero for large  $Q_M$ , while the phase oscillation amplitude goes to zero for slow modulation, and to  $q/Q_M$  for fast modulation. This explains the ‘‘amplitude modulation’’ and ‘‘phase modulation’’ labels in Figure 6. The small angle approximation is only appropriate below the boundary line

$$\left| \frac{qQ_M}{Q_I^2 - Q_M^2} \right| = \frac{1}{5} \quad [69]$$

which is the solid line in Figure 6 showing the resonance pole at  $Q_M = Q_I$ .

Rigorous analysis (see below) shows that this is also the boundary of stability for the  $k=0$  solution in the slow modulation limit. Both simulations and a numerical iterative solution to [64] agree that just below the resonance condition,  $Q_M \leq Q_I$ , this line marks the limit of stability of the  $k=0$  fundamental, but that just above resonance the  $k=0$  solution is stable for all values of  $q$ . This shows that the small angle boundary has different physical implications above and below the resonance. Preliminary results from the numerical iterative solution indicate that none of the  $k \neq 0$  sideband solutions are stable below the resonance [5,7]. In contrast, all of the sideband solutions appear to be stable above resonance, with the possible exception of a small region near the resonance.

Rigorous analysis in the large  $Q_M$  limit (also see below) shows that, although the sidebands may be stable, the size of the islands is insignificant below the small angle boundary. If the sideband islands are big enough to overlap with each other and the fundamental chain of islands, there is large scale chaos. Figure 7 shows the appearance of sideband islands when tune modulation with  $Q_M > Q_I$  is turned on, in the presence of a single beam-beam interaction with a tune shift parameter just below and just above the critical value required for sideband overlap. The two plots on the left do not include tune modulation, while those on the right do. When the tune shift parameter is increased from

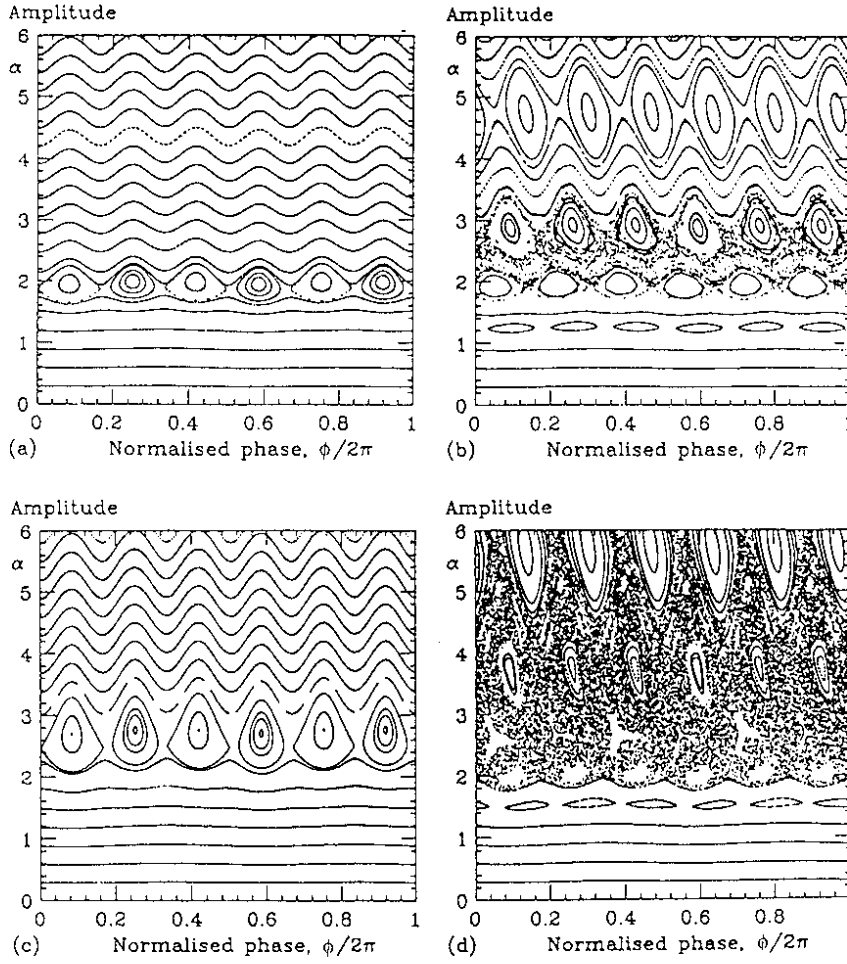


Figure 7. The creation of resonance sidebands, and their chaotic overlap, by tune modulation. A single round beam-beam interaction of strength  $\xi$  perturbs the phase space, with a base tune near a sixth order resonance. Plots a) and b), on top, have  $\xi = 0.0042$ , while the bottom two plots have a slightly stronger value  $\xi = 0.006$ . Plots a) and c), on the left, have no tune modulation, while those on the right have  $(Q_M, q) = (1/194, 0.001)$ . Sidebands become visible when the modulation is turned on in b), but the sidebands must overlap for massive chaos to occur, in d). Amplitude  $\alpha$  is measured in units of the beam size.

$\xi=0.0042$  in the top two plots to  $\xi=0.006$  in the bottom two plots, the sidebands, when they are present, are submerged in a sea of chaos.

Slow modulation — the amplitude modulation region,  $Q_M \ll Q_I$

If the tune is changing so slowly that the motion is adiabatic, it is reasonable to approximate the rate of change as constant. As will be seen, the most stringent conditions come when the rate of change is largest, so the most interesting approximation to the Hamiltonian in equation [61] is

$$H_5 = (2\pi)^2 q Q_M t I + \frac{1}{2} U I^2 - V \cos(5\phi) \quad [70]$$

This Hamiltonian is still time dependent, but now it is possible to go through a canonical coordinate transformation, from  $(I, \phi, H_5)$  to  $(\bar{I}, \bar{\phi}, \bar{H}_5)$ , that produces a time independent Hamiltonian which can be graphically understood. Specifically, the generating function

$$F_3(I, \bar{\phi}, t) = -I\bar{\phi} - \epsilon t \bar{\phi} - \frac{1}{6} \epsilon^2 t^3 \quad [71]$$

with

$$\epsilon = \frac{(2\pi)^2 q Q_M}{U} = 25 V \frac{q Q_M}{Q_I^2} \quad [72]$$

gives, by its definition,

$$\bar{I} \equiv -\frac{\partial F_3}{\partial \bar{\phi}} = I + \epsilon t, \quad \phi \equiv -\frac{\partial F_3}{\partial I} = \bar{\phi} \quad [73]$$

and

$$\bar{H}_5 \equiv H_5 + \frac{\partial F_3}{\partial t} = \frac{1}{2} U \bar{I}^2 - V \cos(5\bar{\phi}) - \epsilon \bar{\phi} \quad [74]$$

While the old phase and the new phase are identical, reflecting the suppression of phase modulation in this region, the new action drifts relative to the old action at a constant speed.

The new Hamiltonian has an extra term, linear in the phase, which has serious consequences for the stability of the  $k=0$  fundamental island chain. (Note that, as a consequence of linearising the rate of change of tune, solutions with  $k \neq 0$  are explicitly impossible in this picture). Pictorially, this non-periodic term corresponds to a constant slope of the quadratic valley of Hamiltonian contours, along the direction of the valley. If this slope is steep enough, there are no longer any local minima. There are minima, and the  $k=0$  solution exists, if there is a solution for the stable fixed point  $(I_{FP}, \phi_{FP})$

$$\begin{pmatrix} \frac{dI}{dt} \\ \frac{d\phi}{dt} \end{pmatrix} = \begin{pmatrix} -5V \sin(5\phi_{FP}) + \epsilon \\ U I_{FP} \end{pmatrix} = \begin{pmatrix} 0 \\ 0 \end{pmatrix} \quad [75]$$

where the overbars have been dropped. If the  $k=0$  islands exist, their centers are at  $I_{FP}=0$ , with a shifted phase. There are no stable islands at all if  $|\epsilon| > 5V$ , that is, if

$$\frac{q Q_M}{Q_I^2} > \frac{1}{5} \quad [76]$$

This condition corresponds, in this limit, to the small angle boundary in equation [69].

Figure 8 shows the effect that crossing this boundary has on the measured lifetime of persistent signals observed in the E778 experiment. A set of symbols of a particular kind corresponds to a single constant value of  $q$ , at a series of  $Q_M$  values. A decay time of 47,000 turns is approximately equivalent to one second in the Tevatron. The decay rate increases dramatically when the stability boundary is crossed, consistent with a fit to the data of  $Q_I = 0.0085$ . Unfortunately, this method of measuring  $Q_I$  is time intensive, since each data point corresponds to a two minute injection cycle of the Tevatron and the analysis is done off-line. It is hoped that in the near future it will be possible to measure  $Q_I$  in a single machine cycle, opening up the possibility of a rapid comprehensive scan of resonances across a relatively wide range of tunes.

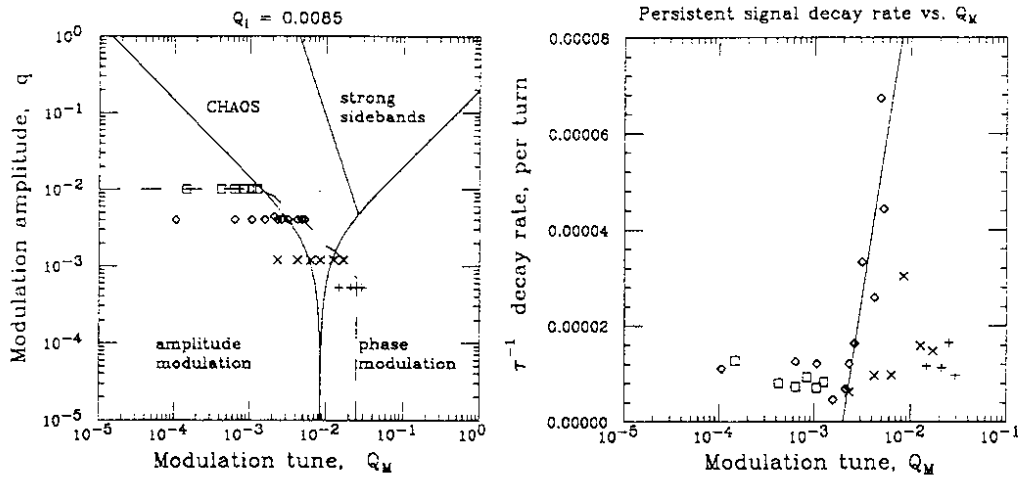


Figure 8. The effect of tune modulation on the decay rate of a persistent signal. Data taken at four values of  $q$  reaches from the amplitude modulation region just into the phase modulation region, and into the chaos region. The decay rate of the persistent signal increases significantly as the boundary between amplitude modulation and chaos is crossed.

Rapid modulation — the phase modulation region,  $Q_M \gg Q_I$

In this region, instead of approximating the old Hamiltonian and then applying a generating function, a time independent Hamiltonian is found by first applying a generating function and then making an approximation. The appropriate generating function is now

$$F_3(I, \bar{\phi}, t) = -I\bar{\phi} - \frac{q}{Q_M} \cos(2\pi Q_M t) I \quad [77]$$

which gives, instead of [73] and [74],

$$\bar{I} = I, \quad \bar{\phi} = \bar{\phi} + \frac{q}{Q_M} \cos(2\pi Q_M t) \quad [78]$$

and

$$\begin{aligned} \bar{H}_5 &= \frac{1}{2} U \bar{I}^2 - V \cos(5\bar{\phi} + \frac{5q}{Q_M} \cos(2\pi Q_M t)) \\ &= \frac{1}{2} U \bar{I}^2 - V \sum_i J_i\left(\frac{5q}{Q_M}\right) \cos(5\bar{\phi} + i 2\pi Q_M t) \end{aligned} \quad [79]$$

where the  $J_i$  are integer order Bessel functions. In this transformation the action remains unchanged, but the phase is modified, appropriate to the phase modulation region. The Hamiltonian is made time independent by concentrating on the vicinity of the  $k$ -th sideband, near an action  $I_k$ , and then averaging the sum in [79] over one modulation period.

In the limit of large  $Q_M$ , not very much happens during one period, and only one turn in the sum survives the averaging. After resynchronising the Hamiltonian to concentrate on the  $k$ -th sideband, and dropping the overbars, then

$$H_{5k} = \frac{1}{2} U (I - I_k)^2 - V J_k\left(\frac{5q}{Q_M}\right) \cos(5\phi) \quad [80]$$

which is time independent, and differs from the simple resonant form [53] mainly by the presence of the  $J_k$  factor. Whether or not the  $k$ -th sideband is significant depends on the value of this Bessel function. As a rule of thumb,  $J_k$  is approximately zero if the absolute value of the argument is less than the absolute value of  $k$ , the order. That is, the sideband  $k$  is only significant if

$$q > |k| \frac{Q_M}{5} \quad [81]$$

The right hand side of this equation is the separation of the sideband tune from the fundamental resonance tune. Equation [81] therefore corresponds to the sensible physical condition that, in order for the resonance to be felt at actions near  $J_k$ , the tune of such trajectories must be modulated far enough to cross the fundamental.

The preceding argument implicitly presumes that the sidebands can be isolated one from the other, and treated separately. This is true if the sideband separation in action,  $(2\pi Q_M)/5U$  according to [67], is larger than the sideband width. If the sidebands are typically wider than they are apart, chaos appears, spanning the action range of the sidebands of significant size. It is easily shown by further approximating the Bessel function, and substituting  $J_k V$  for  $V$  in [58], that sideband overlap is expected if [81] is true, and if

$$Q_M^{3/4} (5q)^{1/4} < \frac{4}{\pi^{1/4}} Q_I \quad [82]$$

This boundary is shown as the second solid line, nearly vertical, in figure 6. Because of the "statistical" approximation of Bessel functions (similar in spirit to approximating a sin function by  $1/\sqrt{2}$ ), this condition is rather qualitative. Depending on the exact phase of the sidebands, some will overlap earlier or later than the condition suggests.

#### ACKNOWLEDGEMENTS AND DEDICATION

Thanks are due to many members of the E778 collaboration for the innumerable contributions they have made, directly and indirectly, to this chapter. Tong Chen has helped to develop the theoretical analysis of tune modulation, and has suffered in helping to prepare the figures, without the reward of visiting the Virgin Islands.

I dedicate this chapter to Maury Tigner, the director of the Central Design Group of the SSC, who is universally admired and respected by the members of the CDG. Without Maury, the SSC would never have become more than a gleam in a physicist's eye.

#### REFERENCES AND FOOTNOTES

1. Poincare, H., *Les methods Nouvelles de la Mechanique Celeste*. Paris: Gautier-Villars. 1892
2. Merminga, N., *A study of nonlinear dynamics in the Fermilab Tevatron*, PhD Thesis, University of Michigan, 1989
3. Edwards and Syphers, *An overview of experiment E778*, Proc of the ICFA workshop, Lugano, 1988
4. Chao et al., *Experimental investigation of nonlinear dynamics in the Fermilab Tevatron*, Physical Review Letters p 2752, December 12, 1988.
5. Chen and Peggs, *Tune modulation and the driven differential pendulum*, to be published in Proc. of the IEEE Particle Accelerator Conference, Chicago, 1989
6. Peggs, Saltmarsh, and Talman, *Million revolution accelerator beam instrument for logging and evaluation*, SSC-169, Berkeley, 1988
7. Peggs, *Hamiltonian theory of the E778 nonlinear dynamics experiment*, SSC-175, Berkeley, 1988

8. Chao et al., A progress report on Fermilab experiment E778, SSC-156, SSC-CDG, Berkeley, 1988
9. Merminga et al., An experimental study of the SSC magnet aperture criterion, Proc. of the EPAC, Rome, 1988
10. Peterson et al., Dynamic aperture measurements at the Tevatron, Proc. of the EPAC, Rome, 1988
11. Landau and Lifshitz, Mechanics, Pergamon press, Oxford, 1976
12. Arnold, V.I., Mathematical methods of classical mechanics, Springer-Verlag, New York, 1978
13. Goldstein, H., Classical mechanics, Addison-Wesley, Menlo Park, 1980
14. Lichtenberg and Lieberman, Regular and stochastic motion, Springer-Verlag, New York, 1983
15. Many accelerator school proceedings (AIP, CERN, or joint CERN/US) are broadly circulated. Their eclectic contents are well worth browsing, both for basic introductions and for specialized topics. Perhaps the two most classic accelerator physics references are Courant and Snyder and Sands, below.
16. Courant and Snyder, Theory of the alternating gradient synchrotron, Annals of Physics:3, 1-48, 1958
17. Sands, M., The physics of electron storage rings, an introduction, SLAC-121, Stanford, 1970
18. Edwards, D., An introduction to circular accelerators, AIP Conf. Proc. No. 127, 1985
19. Peggs and Talman, Nonlinear problems in accelerator physics, Annual Reviews of Nuclear Science, 36:287-325, 1986
20. Ruth, R., Single-particle dynamics in circular accelerators, AIP Conf. Proc. No. 127, 1987
21. Wilson, E., Nonlinear resonances, Proc. of the CERN accelerator school, CERN 87-103, 1987
22. Edwards and Syphers, An introduction to the physics of particle accelerators, AIP Conf. Proc. No. 184, 1988
23. This is hinting at conservation of phase space area, as described by Liouville's theorem. See, for example, Goldstein.
24. Linac designers and constructors claim that they discovered and used strong focussing first, but failed to communicate the knowledge to the accelerator community.
25. SSC Central Design Group, Conceptual design of the Superconducting Super Collider, SSC-SR-2020, Berkeley, 1986
26. Unfortunately there are many slightly different definitions of smear. It is not necessarily possible to convert from one definition to another without making further assumptions about the nature of the motion.
27. Piwinski, A., IEEE Trans. Nucl. Sci. NS-24: 3, 1977
28. Peggs and Talman, Phys Rev D 24: 2379, 1981
29. Myers, S., LEP Note 362, CERN, Geneva, 1982
30. Seeman, J., SLAC-PUB-3182, Palo Alto, Stanford, 1983
31. Keil and Talman, Particle Accelerators 14: 1-2, 109-118, 1983
32. Courant, E., ISABELLE technical note No. 163, Brookhaven, 1980
33. Izrailev, Misnev and Tumaikin, Preprint 77-43, Novosibirsk, 1977
34. Tennyson, J., AIP Conf. Proc. No. 57, New York, 1979
35. Evans and Gareyte, IEEE trans. Nucl. Sci. NS-30: 4, 1982
36. Peggs, Particle Accelerators 17 : 11-50, 1985
37. KAM stands for Kolmogorov, Arnold, and Moser.
38. Moser, J., Nachr. Akad. Wiss. Gottingen, Math. Phys. K1, 1, 1962
39. Siegel and Moser, J. Grund. Math. Wiss. Bd. 187, Springer-Verlag, Berlin, 1971
40. Chirikov, B., Phys. Rep. 52: 265, 1979
41. Henon, M., Appl. Math., No. 3: 291, 1969